Quantification of TSPO overexpression in a rat model of local neuroinflammation induced by intracerebral injection of LPS by the use of [(18)F]DPA-714 PET.

Ory D, Postnov A, Koole M, Celen S, de Laat B, Verbruggen A, Van Laere K, Bormans G, Casteels C.

Published: 1 September 2015

by Springer

in European Journal of Nuclear Medicine and Molecular Imaging

January 2016, Volume 43, Issue 1, pp 163-172

Doi: 10.1007/s00259-015-3172-9

Quantification of TSPO overexpression in a rat model of local neuroinflammation induced by intracerebral injection of LPS by use of [^{18}F]DPA-714 PET

Dieter Ory[a,*], Andrey Postnov[b,*], Michel Koole[b], Sofie Celen[a], Bart de Laat[b], Alfons Verbruggen[a], Koen Van Laere[b], Guy Bormans[a], Cindy Casteels[b]

[a] Laboratory for Radiopharmacy, Department of Pharmaceutical and Pharmacological Sciences, KU Leuven, Leuven, Belgium
[b] Nuclear Medicine and Molecular Imaging, Department of Imaging and Pathology, University Hospital and KU Leuven, Leuven, Belgium

Running title:

TSPO Quantification in Rat Brain

Author for correspondence:

Prof. Guy Bormans, Laboratory for Radiopharmacy, Campus Gasthuisberg O&N2, Herestraat 49 Box 821, BE-3000 Leuven, Belgium. Phone: +32 16 330447; Fax: +32 16 330449; E-mail address: Guy.Bormans@pharm.kuleuven.be

*joint first author

ABSTRACT

Purpose: [^{18}F]DPA-714 is a radiotracer with high affinity for TSPO. We have characterized the kinetics of [^{18}F]DPA-714 in rat brain and evaluated its ability to quantify TSPO expression with PET using a neuroinflammation model induced by unilateral intracerebral injection of lipopolysaccharide (LPS).

Methods: Dynamic small-animal PET scans with [^{18}F]DPA-714 were performed in Wistar rats on a FOCUS-220 system for up to 3 hours. Both plasma and perfused brain homogenates were analyzed using HPLC to quantify radiometabolites. Full kinetic modeling of [^{18}F]DPA-714 brain uptake was performed using a metabolite-corrected arterial plasma input function. Binding potential (BP_{ND}) calculated as Distribution Volume Ratio minus one (DVR-1) between affected and healthy brain tissue was used as outcome measure and evaluated against reference tissue models.

Results: The percentage of intact [^{18}F]DPA-714 in arterial plasma samples was 92±4% at 10 min, 75±8% at 40 min and 52±6% at 180 min. The radiometabolite fraction in brain was negligible (< 3% at 30 min). Among the models investigated, the reversible two-tissue-(2T) compartment model was the most appropriate model to describe [^{18}F]DPA-714 brain kinetics. BP_{ND} values obtained with a Simplified (SRTM) and Multilinear (MRTM) Reference Tissue Model using the contralateral striatum as reference region were in a good correlation (Spearman $r=0.96$; $p\leq0.003$) with 2T BP_{ND} values calculated as DVR-1 and showed comparable bias (% bias range: 17.94, 20.32). Time-stability analysis suggested that acquisition time should be at least 90 min for SRTM and MRTM.

Conclusions: Quantification of [^{18}F]DPA-714 binding to TSPO with full kinetic modeling is feasible using a 2T model. SRTM and MRTM can be suggested as reasonable substitute with

contralateral striatum as reference tissue and scan duration of at least 90 min. However, selection of the reference tissue will be dependent on the disease model used.

Key Words: TSPO, small-animal PET, [^{18}F]DPA-714, kinetic analysis, rat

INTRODUCTION

Tryptophan-rich sensory protein for oxygen (TSPO) receptor [1] or peripheral benzodiazepine receptor (PBR) is the most studied imaging biomarker for neuroinflammation as it is expressed on the outer mitochondrial membrane of microglia [2]. TSPO plays an important role in neurosteroidogenesis, more specifically in the transmembrane transport of cholesterol from the outer to the inner mitochondrial membrane, where the side chain cleavage by cytochrome p450 converts cholesterol into pregnenolone. This pregnenolone is an important precursor for cerebral steroids which play a crucial role in brain development and normal functioning during adulthood [2]. TSPO expression in the central nervous system is low under healthy circumstances. However, TSPO expression increases in response to neuronal insults, mainly in microglia and astrocytes. This can be seen in several neurodegenerative diseases such as Parkinson's disease (PD), Amyotrophic Lateral Sclerosis (ALS), Huntington's disease (HD) and Alzheimer's disease (AD) [2,3]. The exact role of TSPO in regulation of neuroinflammation is not yet fully understood. Bae et al. [4] suggested that TSPO is a negative regulator of neuroinflammation in microglia by attenuation of nuclear factor-kappaB activation and decreased production of pro-inflammatory cytokines. Since the amount of TSPO upregulation in response to injury is correlated with the degree of damage in neuroinflammation, TSPO has been identified as a valuable imaging biomarker for neuroinflammation [5]. [^{11}C]PK11195 has been the most used TSPO PET ligand so far after its introduction in the 80's [6]. Nevertheless, [^{11}C]PK11195 has several limitations such as a high level of non-specific binding and poor signal-to-noise ratios which hamper its quantification. Consequently, new TSPO PET tracers have been designed [2]. One of these radioligands is [^{18}F]DPA-714, developed by James and coworkers [7]. [^{18}F]DPA-714 is reported to have lower non-specific binding and higher affinity for TSPO compared to [^{11}C]PK11195. [^{18}F]DPA-714 has been used in animal models of neuroinflammation [7–10],

in healthy volunteers [11], and in AD [12], stroke [13] and ALS patients [14]. However, kinetic modeling data on [^{18}F]DPA-714 brain uptake in rodents have not been reported so far.

In the present study, we evaluate the quantification of neuroinflammation in rat brain using [^{18}F]DPA-714 small-animal PET. Our primary aim was to compare reference tissue models (RTM) with full kinetic modeling using metabolite-corrected arterial blood input for the [^{18}F]DPA-714 quantification. Our results will indicate whether arterial sampling is needed for an accurate quantification in future studies or whether less invasive approaches provide a valid quantification of [^{18}F]DPA-714 uptake in rodent brain. A rat model of acute, local neuroinflammation induced by lipopolysaccharide (LPS) of gram-negative bacteria was used to evaluate the quantification. LPS activates Toll-like-receptor 4 (TLR4) mainly expressed by macrophages and microglia. Activation of TLR4 induces signal transduction pathways that regulate diverse transcriptional and posttranscriptional processes involved in inflammation [15].

As such, this animal model provides robust, acute, unilaterally neuroinflammation and can therefore be used for screening newly developed PET radiotracers as biomarkers for neuroinflammation and for the evaluation of anti-inflammatory therapies by non-invasive imaging.

MATERIAL AND METHODS

[^{18}F]DPA-714 characteristics and preparation

[^{18}F]DPA-714 was synthesized as previously described [16] with some minor modification, that the HPLC purification was performed using an ethanol-based mobile phase (EtOH:NH_4OAc 10 mM pH 7 35:65 V/V). The final preparation containing less than 10% of EtOH was sterile filtered through a 0.22-µm membrane filter (Millex®-GV, Millipore, Billerica, USA). Radiochemically pure [^{18}F]DPA-714 (> 98%) was obtained with 45-60% yield, relative to starting [^{18}F]F^- radioactivity. The specific activity at the end of synthesis ranged from 149 to 251 GBq/µmol. Precursor and reference compound were kindly provided by Prof. Michael Kassiou (University of Sydney, Australia).

Animals

Experiments were conducted on 10 female Wistar rats (Charles River, France), with an average weight (± standard deviation) of 232±27 g at the start of the experiments. The animals were housed in groups of two, at an average room temperature of 22 °C and a 12-h light/dark cycle. Food and water were given ad libitum.

To induce neuroinflammation, stereotactic surgery was performed three days prior to small-animal PET imaging. All surgical procedures were performed under ketamine (60 mg/kg intraperitoneal (IP) and medetomidine (0.4 mg/kg IP) anesthesia using aseptic procedures. All animals were positioned in a stereotactic head frame (Stoelting, Wood Dale, IL, USA). A small hole was drilled in the skull at the appropriate location using Bregma as reference. Neuroinflammation was induced by injecting 50 µg of lipopolysaccharide (LPS; E. Coli 055:B5; Sigma Aldrich, St. Louis, MO, USA) in 4 µl of sterile 0.9% NaCl solution into the right striatum at the following coordinates: 0.5 mm antero-posterior, 3 mm lateral, 5.5/4.5 mm

dorsoventral. After injection of 2 µl, the needle was retracted dorsoventrally for 1 mm and another 2 µl was injected. The needle was left in place for an additional 10 minutes before being slowly withdrawn from the brain. The contralateral side was injected with 4 µl of sterile 0.9% NaCl solution using an identical procedure.

The research protocol was approved by the local Animal Ethics Committees (P223/2013) and was performed according to European Ethics Committee guidelines (decree 86/609/EEC).

Small-animal PET imaging

Imaging experiments were performed three days after LPS injection on a lutetium oxyorthosilicate detector-based tomograph (microPET FOCUS-220; Siemens Medical Solutions, Malvern, PA, USA), which has a nominative transaxial resolution of 1.35 mm full width at half maximum. The final spatial resolution after rebinning and reconstructing using the specific reconstruction algorithm OSEM 3D followed by MAP was 1.5 mm. Data were acquired in a 128x128x95 matrix with a pixel width of 0.475 mm and a slice thickness of 0.796 mm. The coincidence window width was set at 6 ns.

During PET imaging, rats were kept under gas anesthesia (2.5% isoflurane in O_2 at 1 L/min flow rate), and body temperatures were maintained between 36.5 °C and 37 °C with a heating pad. About 35-54 MBq of [^{18}F]DPA-714 (specific activity range at start PET scan: 81-208 GBq/µmol) was injected into the tail vein using an infusion needle set. Dynamic 180-min acquisitions were started immediately after [^{18}F]DPA-714 injection to assess its kinetics using compartmental modeling.

Acquisition data were Fourier rebinned in 33 frames (4x15, 4x60, 5x180, 8x300, 12x600 s), sinograms were reconstructed using OSEM 3D algorithm followed by MAP (6 iterations, 21 subsets). Corrections were made for attenuation.

Measurement of [^{18}F]DPA-714 in plasma

An arterial cannula was placed in the femoral artery. After slow bolus injection of [^{18}F]DPA-714, arterial blood was continuously collected until 1 min (15 samples, approximately one sample of 40 μL every 4 s allowing detailed (peak) blood input function with high time resolution), followed by 100 μL samples at 90, 120, 150 s and 3, 5, 10, 40, 60, 120 and 180 min. To further prevent possible effects of blood volume changes, we also re-injected 100μL of saline for all samples taken after 90 minutes post injection. This procedure was also helpful for flushing our cannula. All blood samples were immediately stored on ice to stop tracer metabolism. The plasma time-activity curve was corrected for the fraction of unchanged radioligand that was quantified using reversed-phase (RP)-HPLC (LaChrom Elite HPLC system, Hitachi, Darmstadt, Germany; Chromolith C18, 3 mm x 100 mm, Merck, Massachusetts, USA). Plasma samples were isolated from whole blood by centrifugation at 3,000 rpm for 5 min and spiked with standard DPA-714 (20 μg) prior to HPLC analysis (n=6). The HPLC separation was achieved with gradient mixtures of 0.05 M sodium acetate (pH 5.5) (A) and CH_3CN (B) (0-4 min: 100% A, flow rate of 0.5 mL/min; 4.0-4.1 min: 100% A, flow rate of 1 mL/min; and 4.1-14 min; linear gradient from 100% A to 10% A, flow rate of 1.0 mL/min; 14-17 min: 10% A, flow rate of 1 mL/min; 17-25 min: 100% A, flow rate 0.5 mL/min). The HPLC eluate was collected after passing through an inline ultraviolet detector (254 nm) every minute with the exception of every 15 seconds from 1 min before to 1 min after elution of the intact tracer. Radioactivity in all fractions was measured using an automated γ-counter equipped with a 7.62-cm NaI(TI) well crystal coupled to a multichannel analyzer (1480 Wizard; Wallac, Turku, Finland). Results were corrected for background radiation and physical decay during counting.

Measurement of [^{18}F]DPA-714 radiometabolites in brain

Radiometabolites of [^{18}F]DPA-714 in perfused cerebrum and cerebellum of female Wistar rats 3 days after LPS injection (n=3) were quantified at 30 min after tracer injection following a previously described procedure [17] with the difference that the right and left cerebrum were separately evaluated. Brain homogenate extracts were analyzed using an analytical XBridge column (C_{18}, 5 µm, 3 mm x 100 mm; Waters, Milford, USA) eluted with a mixture of 0.01 M ammonium acetate (pH 7) and acetonitrile (67.5:32.5 v/v) at a flow rate of 0.75 mL/min. UV detection was performed at 263 nm.

PET data analysis and kinetic modeling

All PET images were rigidly normalized to a custom-made rat brain template in Paxinos stereotactic space, allowing use of a predefined volume-of-interest map. The procedure of standardization and its validation have been described previously [18].

Time-activity curves for the contralateral (left) and ipsilateral (right) striatum, the contralateral and ipsilateral cortex, and the cerebellum were generated for kinetic modeling with PMOD software (version 3.4; PMOD Technologies, Zurich, Switzerland). Large volume of interest (VOI) were used to improve signal-to-noise ratio [19].

One-tissue (1T) and two-tissue (2T) compartment models including 1T, 2T and 2T with fixed non-displaceable volume (V_{ND}) were considered to describe [^{18}F]DPA-714 kinetics in rat brain using a metabolite-corrected plasma input function. The consensus nomenclature was used according to Innis et al. [20], where V_T is the total distribution volume, including specific and non-displaceable uptake, and BP_{ND} is defined as binding potential representing the ratio between the distribution volumes of specific and non-displaceable binding minus 1.

While modeling the data, we took a region-dependent (variable) blood volume parameter into account. Though TSPO is known to be homogeneously expressed in healthy brain at low levels, we also evaluated different RTMs and reference regions candidates for future quantification without blood sampling. We investigated simplified RTM (SRTM), multilinear RTM (MRTM) [21,22], a two-tissue reference model [23], and standardized uptake value ratios (SUVR) of 10-min scan duration [24]. We used the cerebellum, contralateral (left) striatum and contralateral (left) cortex as potential reference regions. Regions on the contralateral side were chosen because the neuroinflammation remained within the same hemisphere although spread outside the injected striatum was observed (see Fig. 1).

Time stability of BP_{ND} using RTMs was investigated down to a 60-min acquisition, using the value obtained with the complete 180-min dataset as reference.

Statistical analysis

Values are reported as mean ± SD. Conventional statistics were carried out using GraphPad Prism v5.0 (San Diego, CA, USA). The Spearman correlation analysis was used for all correlative tests. Bland-Altman plots were used to test the interchangeability of BP_{ND} values calculated by different methods. Significance was defined at the 95% probability level. Goodness-of-fit by nonlinear least squares analysis was evaluated using the Akaike information criterion (AIC).

RESULTS

Brain kinetics

After injection of [^{18}F]DPA-714, all LPS-treated rats showed highest tracer concentration in the ipsilateral (right) striatum extending towards the ipsilateral cortex. An average PET image (30-180 min) of all rats is shown in Fig. 1. Striatal [^{18}F]DPA-714 uptake values ranged from 0.9 to 1.4 standard uptake value (SUV) after 180 minutes for the affected side and ranged from 0.2 to 0.4 SUV for the non-affected side (Fig. 2A).

Plasma kinetics

The percentage of intact [^{18}F]DPA-714 in arterial plasma over time is shown in Fig. 2B. At 10 min post injection, 91±3% of the total radioactivity in arterial plasma corresponded to [^{18}F]DPA-714. This fraction declined very slowly to 73±8% at 40 min, 56±11% at 120 min and 50±3% at 180 min after tracer injection.

Rat plasma samples contained two radiometabolite fractions, which eluted earlier than [^{18}F]DPA-714 on RP-HPLC and were therefore more hydrophilic (polar) than the parent radioligand (Fig. 2C). No radiometabolites with a higher lipophilicity, i.e. less polar, than [^{18}F]DPA-714 were detected.

Ex vivo radiometabolite analysis in rat brain

Radiometabolite concentration was also quantified in rat brain tissue. Thirty min after tracer injection, the reconstructed radiochromatograms from the HPLC analysis of extracts of right and left cerebrum and cerebellum, showed only one radioactive peak corresponding to intact [^{18}F]DPA-714, eluting at 9 min (chromatograms not shown). For all regions, both the fraction

of more polar and more lipophilic radiometabolites were negligible (< 3%). The recovery of the HPLC (XBridge) column-injected radioactivity was 96.0±2.1% (n=3).

Compartmental modeling of [^{18}F]DPA-714 in rat brain

Compartmental modeling excluded the 1T model from consideration based on Akaike information criterion (AIC) score. The visual quality of the 2T reversible model was also superior to the abovementioned one (Fig.3).

Focusing on the 2T reversible model for describing [^{18}F]DPA-714 brain kinetics, the utility of a fixed non-displaceable distribution volume (2T, fixed V_{ND}) was also evaluated. Fixed V_{ND} was determined using a general 2T model for contralateral striatum, contralateral cortex and cerebellum, and subsequently used for other brain regions. The 2T fixed V_{ND} model was not superior to the 2T model according to AIC, regardless of brain region selected to predetermine the non-displaceable distribution volume. At the same time, non-restricted 2T model resulted in slightly higher V_T values (Table 1). [^{18}F]DPA-714 V_T values of the 2T model were 43.0±19.1 in the ipsilateral striatum, while V_T values of the 2T model were 36.1±14.9, 37.1±15.3, and 37.2±15.1 for the same region, when fixing V_{ND} to the value for the left striatum, cerebellum and left cortex, respectively (not significant, Table 1).

To assess the ability of simplified methods for quantifying tracer binding to TSPO in rats, SRTM and MRTM were evaluated against the 2T model as gold standard using non-displaceable binding potential (BP_{ND}) as the outcome parameter. BP_{ND} of the 2T model using a metabolite-corrected plasma input funtion was calculated as V_T/V_{ref}-1 in which V_{ref} is the distribution volume of the reference region. Different ‘model/reference tissue’ pairs were evaluated.

For both SRTM and MRTM, the contralateral striatum and cerebellum demonstrated excellent correlation between their BP_{ND} values and 2T BP_{ND} (spearman $r > 0.96$, $p \leq 0.003$), while the estimated bias (% bias range: -20.32, 3.64) on Bland-Altman analysis was very limited (Fig. 4). The contralateral cortex was rejected as a candidate to estimate V_{ND} for this tracer, primarily due to BP_{ND} underestimation and high %bias (range: -171.89, -172.53). Interestingly, only when the contralateral striatum was used as reference region in SRTM and MRTM, an additional correlation was observed between its BP_{ND} values and the k3/k4 of 2T (spearman r=1.0; p=0.0004), overall suggesting superiority of this region over the cerebellum as potential reference tissue (Supplementary data Fig. 1). On overview of all statistical comparisons to evaluate 'model/reference tissue' pairs is shown in Table 2. Scatterplots and Bland-Altman plots comparing SRTM and MRTM with both contralateral striatum and cerebellum as reference tissues are shown in Figure 4.

Taking subsequently the contralateral striatum as reference region of choice, SRTM underestimated BP_{ND} by 20.32% and MRTM by 17.94% as compared to 2T. Both SRTM and MRTM did not only demonstrate comparable bias, they also displayed similar 95% limits of agreements, i.e. [-32.49; -8.14] and [-30.18; 5.70] for SRTM and MRTM, respectively, and similar correlation coefficients (both spearman r=0.96; $p \leq 0.003$).

While SRTM and MRTM assume a 1T model as an appropriate model for tracer kinetics of both target and reference region, a 2T model proved to be superior for modeling [^{18}F]DPA-714 kinetics. As a consequence, we also checked whether more sophisticated RT model like the 2T RM would further improve BP_{ND} estimation using a reference region. The 2T RM describes reference tissue kinetics as a 2T model and performed equally good as SRTM and MRTM based on correlation analysis (spearman r=0.94; p=0.003). It showed a smaller underestimation of BP_{ND} (-11.75%), but failed to converge for one animal. In addition, area-under-the-curve based methods like SUVRs at 90, 120 and 180 min all overestimated BP_{ND}

by 8.83±19.44%, 11.01±19.95% and 12.97±20.82%, respectively. They were also highly correlated with the BP_{ND} values of 2T (spearman $r>0.89$; $p<0.05$). However, Bland-Altman analysis of these methods showed an unwanted trend towards a higher bias for longer time windows.

To assess the minimal imaging time required for reliable estimation of BP_{ND}, we gradually reduced the dynamic brain data, from an acquisition interval of 0-180 to an acquisition interval of 0-120, 0-90 and 0-60 minutes. We assessed stability of BP_{ND} estimation over time using both SRTM and MRTM (Fig. 5). The calculated BP_{ND} values increased asymptotically when increasing the scanning interval from 0-60 to 0-180 min. For a 0-90 min scanning interval BP_{ND} estimation using SRTM and MRTM yielded 89% and 90% of the reference value, respectively.

DISCUSSION

The aim of this study was to evaluate different quantification approaches for [^{18}F]DPA-714 uptake in the rat brain injected with LPS. Four reference tissue models were evaluated against full kinetic modeling using metabolite-corrected arterial blood input. In this way, the possibility was assessed to eliminate the need for arterial sampling in rats, hence allowing more straightforward serial [^{18}F]DPA-714 PET measurements over time. We studied the LPS rat model in which a strong TSPO binding had previously been demonstrated [25–27]. In addition, we examined brain and plasma kinetics of [^{18}F]DPA-714, more particularly to which extent radiometabolites are present, pass the BBB and could contribute to specific and/or non-specific binding.

In plasma, two unidentified polar radiometabolite fractions were detected. The radiotracer appeared to be quite stable as at 40 min after radiotracer injection, intact tracer represented 73±8% of the radioactivity in plasma. In brain tissue, the observed fraction of [^{18}F]DPA-714 radiometabolites was negligible in whole cerebrum and cerebellum (<3% of radiometabolites at 30 min after tracer injection), suggesting that this possible confounding factor on the quantification of TSPO binding with PET does not need to be taken into account. This observation is also in line with results presented by Peyronneau and coworkers, who showed that at 120 min post injection, ~85% of activity present in rat brain tissue is still due to intact [^{18}F]DPA-714 [28]. We also observed no difference in the radiometabolite fraction of LPS- and saline- injection cerebrum, indicating limited influence of possible BBB disruption. This was further supported by dynamic Gd-DOTA enhanced magnetic resonance imaging (MRI) in this model showing BBB breakdown near the LPS injection site at day 1, that gradually recovered over time to be almost absent at day 3 post lesioning, i.e. also the timing of our [^{18}F]DPA-714 PET imaging (unpublished findings; supplementary data Fig. 2). Of special

interest was that the detected rate of metabolite formation in plasma was lower in our animal PET study as compared to previous studies with [^{18}F]DPA-714 in rats [28]. This could be due to strain differences in metabolism [29–31]. A possible effect of LPS on the renal and hepatic clearance of drugs (e.g. metformin [32]) is rather limited [33,34], as we injected the LPS stereotactically in the brain.

Among the kinetic models, 1T did not correctly represent [^{18}F]DPA-714 kinetics. A 2T reversible model with metabolite-corrected plasma input was used as the gold standard to evaluate other arterial input models. Reducing the number of parameters from 4 in a 2T reversible model to 3 by fixing the V_{ND} estimate for all brain regions did not result in lower Akaike information criteria values, regardless of brain region that was selected to estimate V_{ND}. This could indicate that the non-displaceable binding cannot be considered as constant throughout the brain, although differences between V_T estimates using a 2T model with fixed V_{ND} and non-restricted one (2T) were very limited. Therefore, the 2T reversible model with 4 parameters is recommended for quantifying [^{18}F]DPA-714 uptake in rat brain, also in line with [^{18}F]DPA-714 findings in humans [12].

Of the investigated reference tissue models, both SRTM and MRTM using the contralateral striatum as reference tissue performed best taking correlative- and Bland-Altman analysis into account. Both RTMs gave comparable bias (~18-20%), displayed similar 95% limits of agreements and correlated well (both spearman r=0.96) with the BP_{ND} given by 2T, indicating that they can be an alternative approach to 2T to circumvent the invasive arterial blood sampling. The reported 18-20% bias likely comes from ignoring the activity in the blood pool as seen in SRTM, combined with the 2T required for describing tissue kinetics [35].

SRTM and MRTM modeling presumes that the reference region is also devoid of receptors and the non-displaceable binding is the same in the reference region, compared with other regions of interest. Unfortunately, expression of TSPO has been reported in the rodent brain both in pathology and non-pathology-related areas [36], albeit at low levels in healthy circumstances. In previous work, the contralateral striatum and cerebellum have been used [37–40] as a reference region for [^{18}F]DPA-714 quantification in rats and humans, but also cluster analysis was performed by several groups [41–43]. Especially in rats, (pre)blocking of TSPO to evaluate the correctness of a reference region has been unsuccessful so far [44].

We have additionally evaluated - in the present study - against full kinetic modeling the use of the contralateral (left) striatum, the cerebellum and the contralateral (left) cortex as reference tissue based on the following rationale: the contralateral striatum was an obvious choice because the level of normal, non-inflammatory expression of TSPO in the mirrored region is expected to be the same as in the LPS-injected one. The drawback was its small size which in case of rat brain leads to noisy time-activity curves. In order to overcome this problem, larger regions like the cerebellum and contralateral (left) cortex were selected to improve signal-to-noise ratios.

Of all reference regions evaluated, results obtained using the contralateral striatum as reference tissue were superior compared to the use of the cerebellum and contralateral cortex. SRTM and MRTM BP_{ND} values using the contralateral striatum did not only correlate with BP_{ND} values of 2T, but also with k3/k4, another parameter expressing binding potential, but one that is characterized in literature by a higher variability as compared to V_T/V_{ref}-1 [12,45,46]. Also, using the cerebellum as reference region, we reported lower BP_{ND} values upon [^{18}F]DPA-714 quantification with greater variability on Bland-Altman analysis, despite a nearly perfect correlation; overall suggesting a higher bias of specific binding in this region as compared to the contralateral striatum. Specific binding in the cerebellar area has already

previously been reported around the ventricles for both rat en monkey brain [5,47]. This was also seen when Feng and coworkers used [^{123}I]-CLINDE to image TSPO in patients with stroke and glioblastoma. They reported that cerebellar V_T values fall into categories determined by the three TSPO genotypes [48]. In our work, the contralateral cortex turned out to be not a good candidate to define $V_{ND,}$ as reflected by the high underestimation and high bias (%range: -171.89, -172.53) probably due to partial volume effects of the relatively high TSPO binding in the harderian glands and bulbus olfactorius [49].

The unilateral LPS injection model and the corresponding focal inflammation facilitated the choice of an appropriate reference tissue. However, for other models of neuroinflammation where inflammation is expected to be less focal, the choice of an appropriate reference tissue needs careful consideration. Therefore, methodologies which have been developed for automatically extracting reference tissue input curves for human brain PET studies with (R)-[^{11}C]PK11195 should be considered for translation into a preclinical setting [41]. This way, reference tissue models could be applied without any presumption about the location of the brain inflammation and without relying on focal inflammation.

Reduction of the scanning time is desirable for experiment simplicity, for cost effectiveness and for diminishing anesthesia effects on diseased animals. Quantification of the [^{18}F]DPA-714 binding as BP_{ND} using SRTM and MRTM did not provide stable values below 90 minutes of scan duration. The more appropriate 2T RT model which takes into account a 2T model for reference tissue kinetics did reduce the BP_{ND} bias of SRTM and MRTM compared to BP_{ND} estimates with an unconstrained 2T model. However, the model failed for one animal, probably due to the fact that tracer kinetics of that specific animal was close to 1T kinetics. Therefore, a 2T RT model is not considered the model of choice for quantifying [^{18}F]DPA-714 with a reference tissue model.

In terms of SUVR quantification, we observed a systematic overestimation of TSPO binding compared to BP_{ND} values estimated with an unconstrained 2T model with the degree of overestimation increasing with later time windows. This bias is very similar to the bias observed with SUVR for the quantification of [^{11}C]-PIB brain PET data and can be caused as a result of plasma clearance [50]. Therefore, SUVR cannot be considered as a good approximation of DVR.

From a methodological point-of-view, we believe that the 2T model used in this manuscript to quantify TSPO binding in rats, will also remain the model of choice for assessing low-grade inflammation using [^{18}F]DPA-714 in other chronic rat models. One may only expect in rat models of low-grade inflammation more noise in the target region, but this effect can be reduced by taking larger volumes-of-interest to improve the signal-to-noise ratio. However, whether [^{18}F]DPA-714 will eventually be able to detect this low degree of inflammation still remains unclear, and was not our aim to evaluate in this manuscript. Nevertheless, Lavisse and coworkers recently quantified the amount of TSPO on brain sections of QA injected monkeys using immunohistochemistry and compared it to [^{18}F]DPA-714 PET imaging [47]. One major advantage of their QA model is that the activation process (microglial activation accompanied by a late progressive astrocytic reaction) progresses over several months, which enables the longitudinal analysis of each glial activation phase in vivo. They reported that changes in specific binding only became statistically significant in the lesion on day 21 (2.7-fold increase in V_T), associated with an increase in TSPO optical density by 7.6-fold. They thus suggested that a relatively large change in TSPO density must occur in the diseased brain in order to be detected in vivo by [^{18}F]DPA-714 PET imaging, having implications for the detection of low-grade inflammation in disorders such as Alzheimer's disease, Huntington's disease and Parkinson's disease.

CONCLUSION

In conclusion, we successfully characterized the kinetics of [^{18}F]DPA-714 in rat brain. Two radiometabolite fractions are present in plasma, but there was no evidence suggesting that these cross the blood-brain-barrier. Full quantification of the tracer binding to TSPO was possible using a 2T model. SRTM and MRTM with the contralateral striatum as reference tissue are reasonable substitutes to circumvent the invasive arterial blood sampling provided that an acquisition time of at least 90 minutes is retained.

ACKNOWLEDGEMENTS

Dieter Ory is a fellow of the Research Foundation Flanders (FWO). This research is funded by the European Union's Seventh Framework Programme (FP7/2007-2013) under grant agreement n° HEALTH-F2-2011-278850 (INMiND). Cindy Casteels is a postdoctoral Research Fellow of FWO. Koen Van Laere is senior clinical researcher of FWO. We would like to thank Julie Cornelis and Ann Van Santvoort for their excellent assistance in the animal work.

CONFLICT OF INTEREST

The authors declare that they have no conflict of interest.

ETHICAL APPROVAL

All applicable international, national, and/or institutional guidelines for the care and use of animals were followed.

REFERENCES

1. Yeliseev AA, Kaplan S. A Sensory Transducer Homologous to the Mammalian Peripheral-type Benzodiazepine Receptor Regulates Photosynthetic Membrane Complex Formation in Rhodobacter sphaeroides 2.4.1. J Biol Chem 1995;270:21167–75.

2. Ory D, Celen S, Verbruggen A, Bormans G. PET Radioligands for In Vivo Visualization of Neuroinflammation. Curr Pharm Des 2014;20:5897–913.

3. Venneti S, Wiley CA, Kofler J. Imaging microglial activation during neuroinflammation and Alzheimer's disease. J Neuroimmune Pharmacol 2009;4:227–43.

4. Bae K-R, Shim H-J, Balu D, Kim SR, Yu S-W. Translocator protein 18 kDa negatively regulates inflammation in microglia. J Neuroimmune Pharmacol 2014;9:424–37.

5. Chen M-K, Guilarte TR. Translocator protein 18 kDa (TSPO): molecular sensor of brain injury and repair. Pharmacol Ther 2008;118:1–17.

6. Le Fur G, Perrier ML, Vaucher N, et al. Peripheral benzodiazepine binding sites: effect of PK 11195, 1-(2-chlorophenyl)-N-methyl-N-(1-methylpropyl)-3-isoquinolinecarboxamide. I. In vitro studies. Life Sci 1983;32:1839–47.

7. James ML, Fulton RR, Vercoullie J, et al. DPA-714, a new translocator protein-specific ligand: synthesis, radiofluorination, and pharmacologic characterization. J Nucl Med 2008;49:814–22.

8. Boutin H, Prenant C, Maroy R, et al. [^{18}F]DPA-714: direct comparison with [^{11}C]PK11195 in a model of cerebral ischemia in rats. PLoS One 2013;8:e56441.

9. Chauveau F, Van Camp N, Dollé F, et al. Comparative evaluation of the translocator protein radioligands ^{11}C-DPA-713, ^{18}F-DPA-714, and ^{11}C-PK11195 in a rat model of acute neuroinflammation. J Nucl Med 2009;50:468–76.

10. Harhausen D, Sudmann V, Khojasteh U, et al. Specific imaging of inflammation with the 18 kDa translocator protein ligand DPA-714 in animal models of epilepsy and stroke. PLoS One 2013;8:e69529.

11. Arlicot N, Vercouillie J, Ribeiro M-J, et al. Initial evaluation in healthy humans of [^{18}F]DPA-714, a potential PET biomarker for neuroinflammation. Nucl Med Biol 2012;39:570–8.

12. Golla SS V, Boellaard R, Oikonen V, et al. Quantification of [(^{18})F]DPA-714 binding in the human brain: initial studies in healthy controls and Alzheimer's disease patients. J Cereb Blood Flow Metab 2015; 35:766-72.

13. Ribeiro M-J, Vercouillie J, Debiais S, et al. Could (^{18}) F-DPA-714 PET imaging be interesting to use in the early post-stroke period? EJNMMI Res 2014;4:28.

14. Corcia P, Tauber C, Vercoullie J, et al. Molecular imaging of microglial activation in amyotrophic lateral sclerosis. PLoS One 2012;7:e52941.

15. Glass CK, Saijo K, Winner B, Marchetto MC, Gage FH. Mechanisms underlying inflammation in neurodegeneration. Cell 2010;140:918–34.

16. Damont A, Hinnen F, Kuhnast B, et al. Radiosynthesis of [^{18}F]DPA-714, a selective radioligand for imaging the translocator protein (18 kDa) with PET. J Label Compd Radiopharm 2008;51:286–92.

17. Ooms M, Celen S, Koole M, et al. Synthesis and biological evaluation of carbon-11 and fluorine-18 labeled tracers for in vivo visualization of PDE10A. Nucl Med Biol 2014;41:695–704.

18. Casteels C, Vermaelen P, Nuyts J, et al. Construction and evaluation of multitracer small-animal PET probabilistic atlases for voxel-based functional mapping of the rat brain. J Nucl Med 2006;47:1858–66.

19. Tai Y-C, Ruangma A, Rowland D, et al. Performance evaluation of the microPET focus: a third-generation microPET scanner dedicated to animal imaging. J Nucl Med 2005;46:455–63.

20. Innis RB, Cunningham VJ, Delforge J, et al. Consensus nomenclature for in vivo imaging of reversibly binding radioligands. J Cereb Blood Flow Metab 2007;27:1533–9.

21. Lammertsma AA, Hume SP. Simplified reference tissue model for PET receptor studies. Neuroimage 1996;4:153–8.

22. Ichise M, Liow J-S, Lu J-Q, et al. Linearized reference tissue parametric imaging methods: application to [^{11}C]DASB positron emission tomography studies of the serotonin transporter in human brain. J Cereb Blood Flow Metab 2003;23:1096–112.

23. Millet P, Graf C, Buck A, Walder B, Ibáñez V. Evaluation of the reference tissue models for PET and SPECT benzodiazepine binding parameters. Neuroimage 2002;17:928–42.

24. McNamee RL, Yee S-H, Price JC, et al. Consideration of optimal time window for Pittsburgh compound B PET summed uptake measurements. J Nucl Med 2009;50:348–55.

25. Dickens AM, Vainio S, Marjamäki P, et al. Detection of microglial activation in an acute model of neuroinflammation using PET and radiotracers ^{11}C-(R)-PK11195 and ^{18}F-GE-180. J Nucl Med 2014;55:466–72.

26. Moon BS, Kim BS, Park C, et al. [(^{18})F]Fluoromethyl-PBR28 as a potential radiotracer for TSPO: preclinical comparison with [(^{11})C]PBR28 in a rat model of neuroinflammation. Bioconjug Chem 2014;25:442–50.

27. Ory D, Planas A, Dresselaers T, et al. PET imaging of TSPO in a rat model of local neuroinflammation induced by intracerebral injection of lipopolysaccharide. Nucl Med Biol 2015; In Press

28. Peyronneau M-A, Saba W, Goutal S, et al. Metabolism and quantification of [(^{18})F]DPA-714, a new TSPO positron emission tomography radioligand. Drug Metab Dispos 2013;41:122–31.

29. Morita K, Maeda Y, Masuda M, et al. Strain Differences in CYP3A-Mediated C-8 Hydroxylation (1,3,7-Trimethyluric Acid Formation) of Caffeine in Wistar and Dark Agouti Rats. Biochem Pharmacol 1998;55:1405–11.

30. Tanoue C, Sugihara K, Uramaru N, et al. Strain difference of oxidative metabolism of the sedative-hypnotic zaleplon by aldehyde oxidase and cytochrome P450 in vivo and in vitro in rats. Drug Metab Pharmacokinet 2013;28:269–73.

31. Saito K, Sakai N, Kim H-S, Ishizuka M, Kazusaka A, Fujita S. STRAIN DIFFERENCES IN DIAZEPAM METABOLISM AT ITS THREE METABOLIC SITES IN SPRAGUE-DAWLEY, BROWN NORWAY, DARK AGOUTI, AND WISTAR STRAIN RATS. Drug Metab Dispos 2004;32:959–65.

32. Cho YK, Choi YH, Kim SH, Lee MG. Effects of Escherichia coli lipopolysaccharide on the metformin pharmacokinetics in rats. Xenobiotica 2009;39:946–54.

33. Hasegawa T, Takagi K, Kitaichi K. Effects of bacterial endotoxin on drug pharmacokinetics. Nagoya J Med Sci 1999;62:11–28.

34. Yang KH, Lee MG. Effects of endotoxin derived from Escherichia coli lipopolysaccharide on the pharmacokinetics of drugs. Arch Pharm Res 2008;31:1073–86.

35. Salinas CA, Searle GE, Gunn RN. The simplified reference tissue model: model assumption violations and their impact on binding potential. J Cereb Blood Flow Metab 2015;35:304–11.

36. Tang D, Hight MR, McKinley ET, et al. Quantitative preclinical imaging of TSPO expression in glioma using N,N-diethyl-2-(2-(4-(2-^{18}F-fluoroethoxy)phenyl)-5,7-dimethylpyrazolo[1,5-a]pyrimidin-3-yl)acetamide. J Nucl Med 2012;53:287–94.

37. Groom GN, Junck L, Foster NL, Frey KA, Kuhl DE. PET of peripheral benzodiazepine binding sites in the microgliosis of Alzheimer's disease. J Nucl Med 1995;36:2207–10.

38. Banati RB, Goerres GW, Myers R, et al. [^{11}C](R)-PK11195 positron emission tomography imaging of activated microglia in vivo in Rasmussen's encephalitis. Neurology 1999;53:2199–203.

39. Versijpt JJ, Dumont F, Van Laere KJ, et al. Assessment of neuroinflammation and microglial activation in Alzheimer's disease with radiolabelled PK11195 and single photon emission computed tomography. A pilot study. Eur Neurol 2003;50:39–47.

40. Gerhard A, Schwarz J, Myers R, Wise R, Banati RB. Evolution of microglial activation in patients after ischemic stroke: a [^{11}C](R)-PK11195 PET study. Neuroimage 2005;24:591–5.

41. Yaqub M, van Berckel BNM, Schuitemaker A, et al. Optimization of supervised cluster analysis for extracting reference tissue input curves in (R)-[(^{11})C]PK11195 brain PET studies. J Cereb Blood Flow Metab 2012;32:1600–8.

42. Schuitemaker A, Kropholler MA, Boellaard R, et al. Microglial activation in Alzheimer's disease: an (R)-[^{11}C]PK11195 positron emission tomography study. Neurobiol Aging 2013;34:128–36.

43. Banati RB, Newcombe J, Gunn RN, et al. The peripheral benzodiazepine binding site in the brain in multiple sclerosis: quantitative in vivo imaging of microglia as a measure of disease activity. Brain 2000;123 (Pt 1:2321–37.

44. Doorduin J, Klein HC, Dierckx RA, James M, Kassiou M, de Vries EFJ. [^{11}C]-DPA-713 and [^{18}F]-DPA-714 as new PET tracers for TSPO: a comparison with [^{11}C]-(R)-PK11195 in a rat model of herpes encephalitis. Mol Imaging Biol 11:386–98.

45. Lammertsma AA, Bench CJ, Hume SP, et al. Comparison of methods for analysis of clinical [^{11}C]raclopride studies. J Cereb Blood Flow Metab 1996;16:42–52.

46. Yaqub M, Boellaard R, van Berckel BNM, et al. Evaluation of tracer kinetic models for analysis of [^{18}F]FDDNP studies. Mol Imaging Biol 11:322–33.

47. Lavisse S, Inoue K, Jan C, et al. [^{18}F]DPA-714 PET imaging of translocator protein TSPO (18 kDa) in the normal and excitotoxically-lesioned nonhuman primate brain. Eur J Nucl Med Mol Imaging 2015;42:478–94.

48. Feng L, Svarer C, Thomsen G, et al. In vivo quantification of cerebral translocator protein binding in humans using 6-chloro-2-(4'-123I-iodophenyl)-3-(N,N-diethyl)-imidazo[1,2-a]pyridine-3-acetamide SPECT. J Nucl Med 2014;55:1966–72.

49. Dedeurwaerdere S, Callaghan PD, Pham T, et al. PET imaging of brain inflammation during early epileptogenesis in a rat model of temporal lobe epilepsy. EJNMMI Res 2012;2:60.

50. Carson RE, Channing MA, Blasberg RG, et al. Comparison of bolus and infusion methods for receptor quantitation: application to [^{18}F]cyclofoxy and positron emission tomography. J Cereb Blood Flow Metab 1993;13:24–42.

TABLES

Table 1: Distribution volume of the LPS-injected striatum with two-tissue reversible model with and without V_{ND} fixed at contralateral (left) striatum, cerebellum and contralateral (left) cortex

Distribution volume (V_T)				
	2T	2T, fixed V_{ND} [contralateral striatum]	2T, fixed V_{ND} [cerebellum]	2T, fixed V_{ND} [contralateral cortex]
rat #1	19.2	18.4	18.8	18.7
rat #2	20.8	19.9	19.9	20.2
rat #3	53.0	42.7	43.2	43.4
rat #4	52.6	42.1	45.6	45.5
rat #5	69.7	59.6	60.8	60.1
rat #6	53.7	42.6	42.8	43.6
rat #7	32.3	27.4	28.3	28.7

Region between [] refers to the reference tissue used

Table 2. Statistical comparison of Reference Tissue Models (RTM) for [^{18}F]-DPA-714 versus 2T

	BP_{ND} of Right Striatum	Spearman Rho	Bland-Altman %Bias [95% limits of agreement])
$SRTM_{[Left\ Striatum]}$	3.00±1.06	0,96**	-20.32% [-32.49; -8.14]
$MRTM_{[Left\ Striatum]}$	3.05±1.06	0,96**	-17.94% [-30.18; -5.70]
$SRTM_{[Cerebellum]}$	1.49±0.57	1,000***	3.64% [-86.08; 93.36]
$MRTM_{[Cerebellum]}$	1.50±0.62	1,000***	-16.70% [-140,75; 107.35]
$SRTM_{[Left\ Cortex]}$	1.61±0.76	0,93**	-171.89% [-281.72; -62.07]
$MRTM_{[Left\ Cortex]}$	1.61±0.78	0,96**	-172.53% [-283.24; -61.81]
2T reference $model_{[Left\ Striatum]}$	3.53±1.72	0,94*	-11.75% [-30.50; 7.00]
180 min $SUVR_{[Left\ Striatum]}$	4.24±1.33	0,89*	12.97% [-27.84; 53.78]
120 min $SUVR_{[Left\ Striatum]}$	4.12±1.17	0,96**	11.01% [-27.09; 49.12]
90 min $SUVR_{[Left\ Striatum]}$	3.94±1.04	0,96**	8.33% [-30.78; 47.43]

Region between [] refers to the reference tissue used
*p<0.05; **p<0.01; ***p<0.001

FIGURES LEGENDS

Figure 1: Mean [^{18}F]DPA-714 distribution in rat brain. Average cross-sectional small-animal PET images of [^{18}F]DPA-714 uptake in rat brain from 30 to 180 min (n=7). The colored bar expresses SUV. The intersection point of the three planes have been set to the mid-striatal level (i.e. (x,y,z)=(-2.9, -0.3, -5.6) Paxinos coordinates), which corresponds to the right hemisphere.

Figure 2: Brain and plasma kinetics of [^{18}F]DPA-714 in rat. (a) Average time-activity curves of [^{18}F]DPA-714 for different brain regions in rat, unilaterally lesioned with LPS (n=7). Concentration is expressed as standardized uptake value (SUV), which normalizes for injected radioactivity and body weight. **(b)** Average percentage of intact [^{18}F]DPA-714 in arterial plasma samples of rats scanned for 180 min. Data are expressed as mean ± SD (n=7). **(c)** Reconstructed radiochromatograms of rat plasma analysis after [^{18}F]DPA-714 injection (n=1). Two polar radiometabolite(s) fractions are detectable. n° = number.

Figure 3: One-tissue and two-tissue compartment analysis with radiometabolite-corrected plasma input. Representative fits of the rat brain [18F]DPA-714 time-activity-curve for ipsilateral (right) striatum (a), contralateral (left) striatum (b) and cerebellum (c) using a one-tissue compartment model *(dashed lines)* and two-tissue reversible compartment model *(solid lines)*.

Figure 4: Scatterplots *(top row)* and Bland-Altman plots *(bottom row)* of BP_{ND} values of SRTM vs. 2T *(a-c)* and of MRTM vs. 2T *(b-d)* using both the contralateral striatum *(a-b)* and cerebellum *(c-d)* as reference tissue. Bland-Altman plots give difference of BP_{ND} between two models in logarithmic scale vs. average BP_{ND}. 95% limits of agreement are given in *dotted line* and average difference in *solid line*.

Figure 5: Time stability of binding potential values (BP_{ND}) in rat Increasingly truncated intervals of brain time-activity data were analyzed from 0 to 180 min. BP_{ND} was calculated for SRTM (□) and MRTM (Δ) and expressed as a ratio to that determined with the complete scanning from 0 to 180 min. The error bar represents SD of the ratios, n=7 animals.

SUPPLEMENTARY DATA

Figure 1: Scatterplots of BP_{ND} values of SRTM vs. 2T k3/k4 using the contralateral striatum *(full circles)* and cerebellum *(triangles)* as reference tissue. Note that BP_{ND} values of SRTM only correlated with 2T k3/k4 when the contralateral (left) striatum was used as reference tissue.

Figure 2: Dynamic Gd-DOTA enhanced magnetic resonance imaging (MRI) in LPS-treated rats (a) Illustration of the relative contrast enhancement (RCE) resulting from the Gd-DOTA injection at different time points after LPS and saline injection, i.e. 1 day, 3 days, 1 week and 1 month. BBB disruption near the LPS injection site (right hemisphere) is evident at 1 day and reduced at 3 and 7 days. No contrast enhancement is seen 1 month after the LPS injection or near the saline injection site (left hemisphere; all time points). (b) No [^{18}F]DPA-714 uptake is seen when BBB disruption is maximal at day 1 while specific tracer binding is observed in the LPS injected striatum at day 3 when BBB almost recovered totally. This suggests that [^{18}F]DPA-714 binding at day 3 is limited biased by BBB disruption.

Figure 1

Click here to download Figure: DOry Figure 1 Eur J Nucl Med Mol Imaging.tif

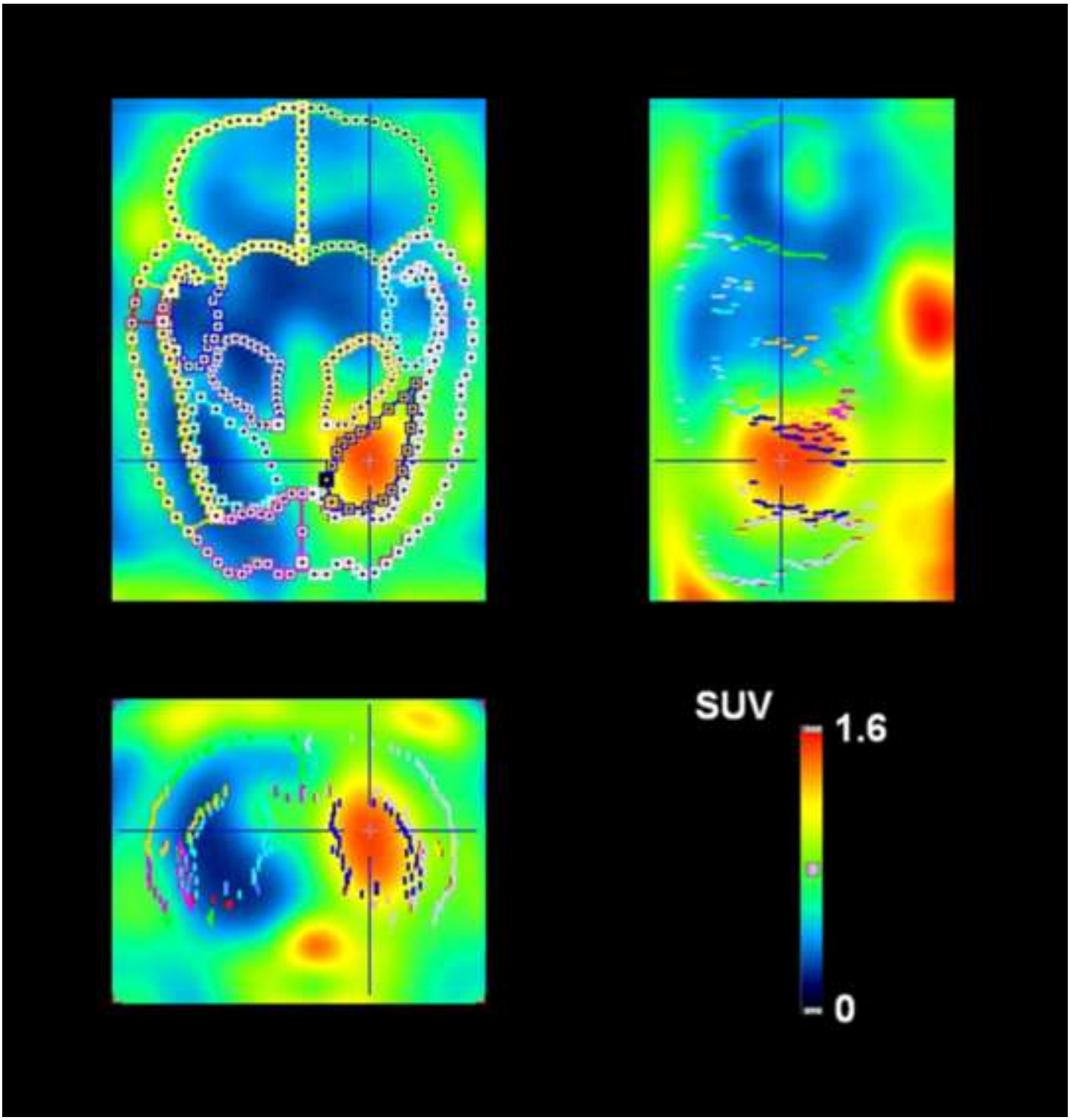

Figure 2

Click here to download Figure: DOry Figure 2 Eur J Nucl Med Mol Imaging.tif

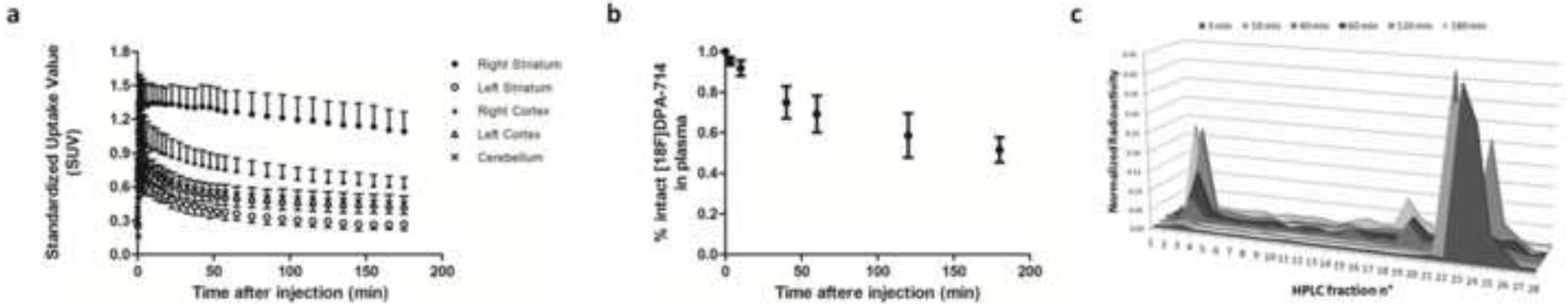

Figure 3

Click here to download Figure: DOry Figure 3 Eur J Nucl Med Mol Imaging.tif

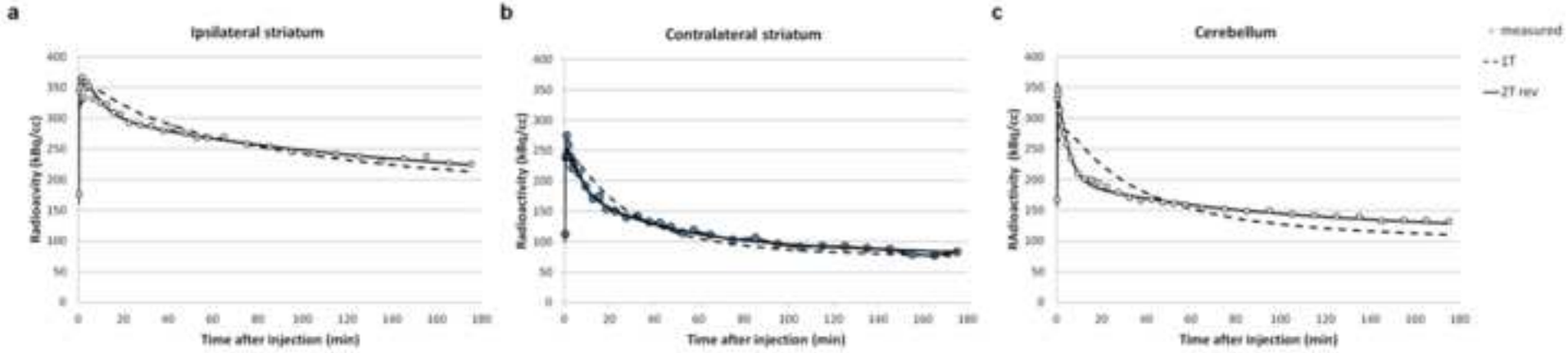

Figure 4

Click here to download Figure: DOry Figure 4 Eur J Nucl Med Mol Imaging.tif

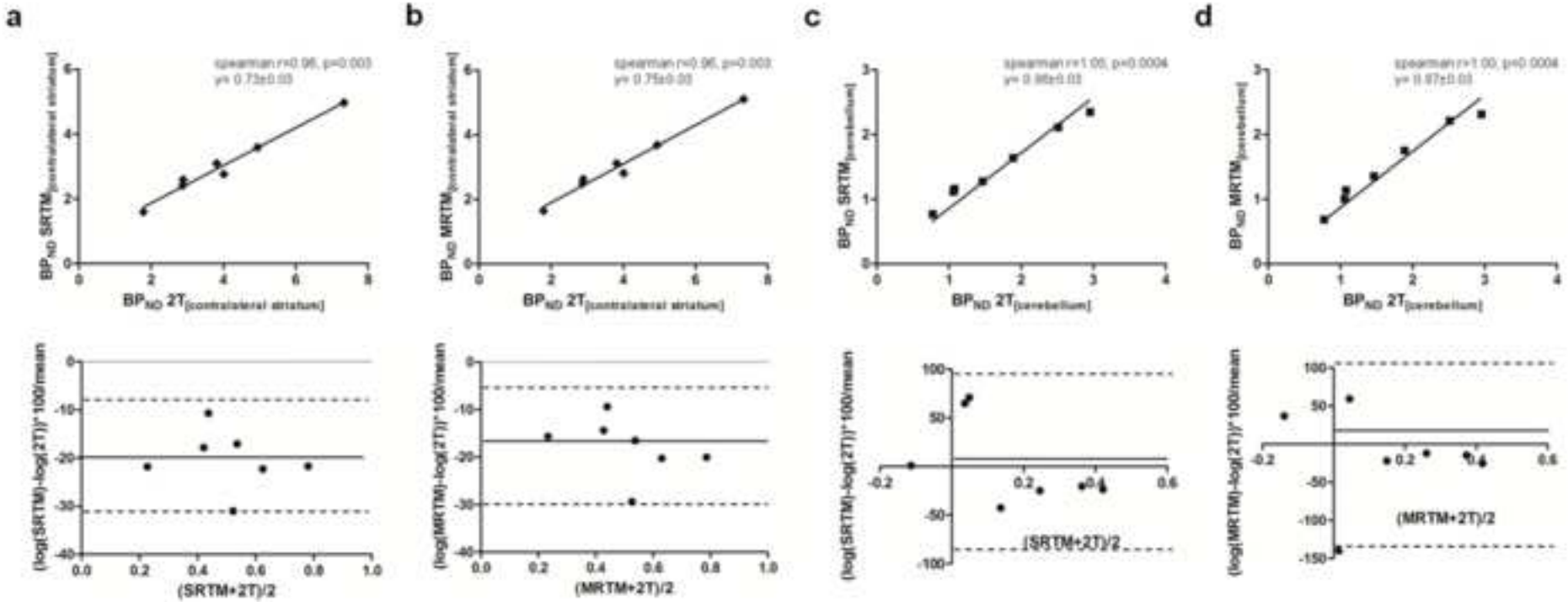

Figure 5

Click here to download Figure: DOry Figure 5 Eur J Nucl Med Mol Imaging.tif

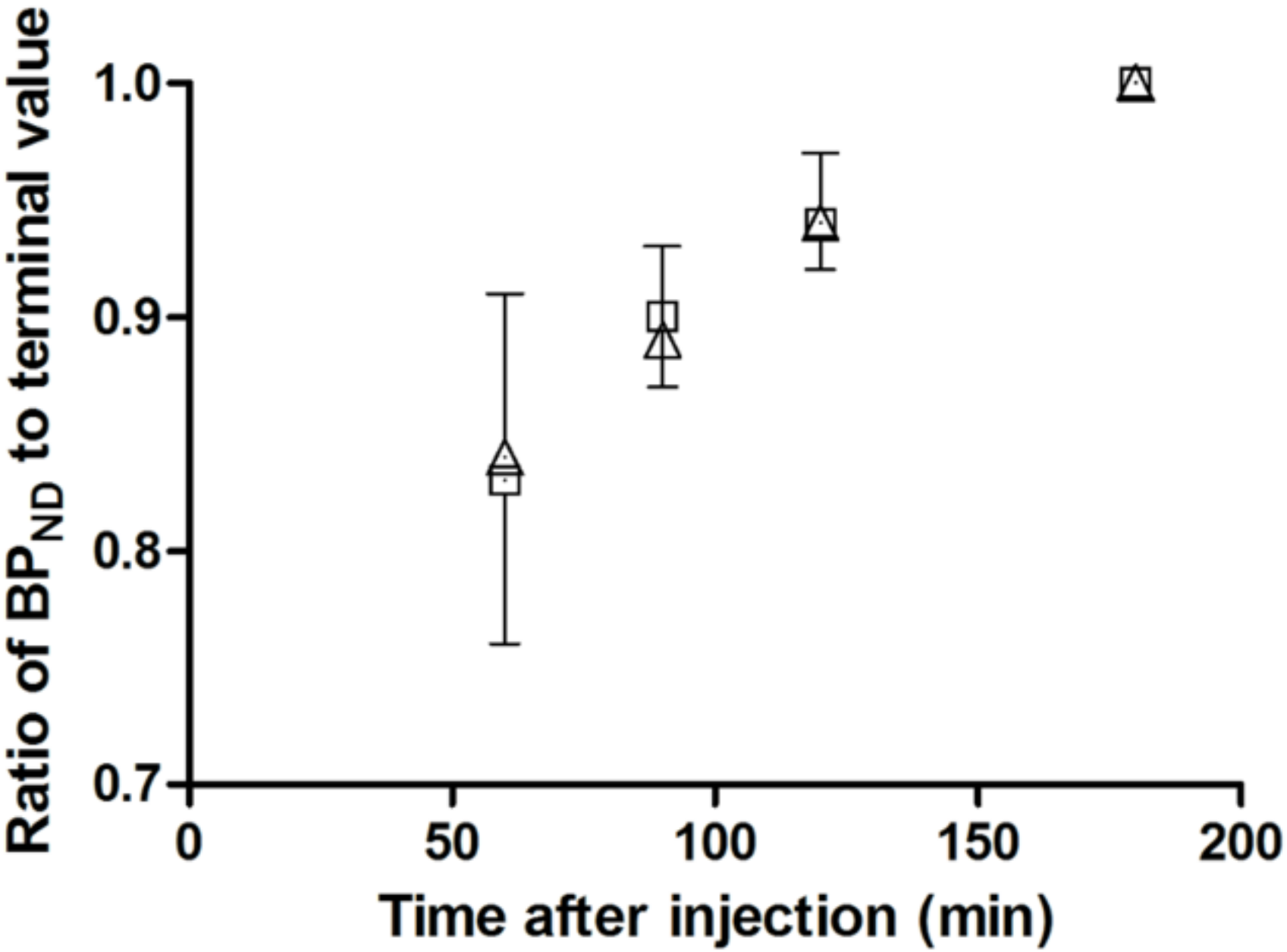

Supplementary Material Figure 1

Click here to download Supplementary Material: DOry Suppl Figure 1 Eur J Nucl Med Mol Imaging.tif

Supplementary Material Figure 2

Click here to download Supplementary Material: DOry Suppl Figure 2 Eur J Nucl Med Mol Imaging.tif

Table 1: Distribution volume of the LPS-injected striatum with two-tissue reversible model with and without V_{ND} fixed at contralateral (left) striatum, cerebellum and contralateral (left) cortex

Distribution volume (V_T)				
	2T	2T, fixed V_{ND} [contralateral striatum]	2T, fixed V_{ND} [cerebellum]	2T, fixed V_{ND} [contralateral cortex]
rat #1	19.2	18.4	18.8	18.7
rat #2	20.8	19.9	19.9	20.2
rat #3	53.0	42.7	43.2	43.4
rat #4	52.6	42.1	45.6	45.5
rat #5	69.7	59.6	60.8	60.1
rat #6	53.7	42.6	42.8	43.6
rat #7	32.3	27.4	28.3	28.7

Region between [] refers to the reference tissue used

Table 2

Table 2. Statistical comparison of Reference Tissue Models (RTM) for [^{18}F]-DPA-714 versus 2T

	BP_{ND} of Right Striatum	Spearman Rho	Bland-Altman %Bias [95% limits of agreement])
$SRTM_{[Left\ Striatum]}$	3.00±1.06	0,96**	-20.32% [-32.49; -8.14]
$MRTM_{[Left\ Striatum]}$	3.05±1.06	0,96**	-17.94% [-30.18; -5.70]
$SRTM_{[Cerebellum]}$	1.49±0.57	1,000***	3.64% [-86.08; 93.36]
$MRTM_{[Cerebellum]}$	1.50±0.62	1,000***	-16.70% [-140,75; 107.35]
$SRTM_{[Left\ Cortex]}$	1.61±0.76	0,93**	-171.89% [-281.72; -62.07]
$MRTM_{[Left\ Cortex]}$	1.61±0.78	0,96**	-172.53% [-283.24; -61.81]
2T reference $model_{[Left\ Striatum]}$	3.53±1.72	0,94*	-11.75% [-30.50; 7.00]
180 min $SUVR_{[Left\ Striatum]}$	4.24±1.33	0,89*	12.97% [-27.84; 53.78]
120 min $SUVR_{[Left\ Striatum]}$	4.12±1.17	0,96**	11.01% [-27.09; 49.12]
90 min $SUVR_{[Left\ Striatum]}$	3.94±1.04	0,96**	8.33% [-30.78; 47.43]

Region between [] refers to the reference tissue used
*p<0.05; **p<0.01; ***p<0.001